ON THE MODELLING OF BUBBLE ENTRAINMENT BY IMPINGING JETS IN CFD-SIMULATIONS

M. Schmidtke, D. Lucas

Forschungszentrum Dresden-Rossendorf, Germany
P.O. Box 51 01 19, 01314 Dresden
M.Schmidtke@fzd.de, D.Lucas@fzd.de

Abstract This contribution presents different approaches for the modeling of air entrainment under water by plunging jets in CFD codes. In simulations which include the full length of the jet and its environment, the process of bubble generation can not be resolved due to computational limitations. This is why the air entrainment has to be modeled in meso-scale simulations. In the frame of an Euler-Euler simulation, the local morphology of the phases has to be considered in the drag model. In the impinging jet configuration, the air is a continuous phase above the water level but bubbly below the water level. Various drag models are implemented in the CFD solver CFX11 and their influence on the gas void fraction below the water level is discussed. The algebraic interface area density (AIAD) model applies a drag coefficient for bubbles and a different drag coefficient for the free surface. If the AIAD model is used for the simulation of impinging jets, the gas entrainment depends on the free parameters included in this model. The calculated gas entrainment can be adapted via these parameters. Therefore, an advanced AIAD approach could be used in future for the implementation of models (e.g. correlations) for the gas entrainment.

1. INTRODUCTION

The configuration of an impinging jet occurs in different scenarios of reactor safety analysis. In the scenario of an emergency core cooling (ECC) water is injected into the cold leg. Some loss of coolant accident scenarios assume that the cold leg pipe is only partially filled with hot water. In this case, the injected cold water impinges as a jet on the surface of the hot water. Depending on the velocity of the jet, steam bubbles may be entrained below the surface by the impinging jet. These bubbles contribute to heat exchanged and mixing of the fluids. Heat transfer between cold and hot water and mixing in the cold leg plays an important role since the mixed water enters the reactor pressure vessel and may cause high temperature gradients at the wall of the vessel. These gradients cause mechanical stress in the wall due to thermal shock, which can have a negative effect on the durability of the reactor vessel.

An impinging jet may also occur, when an emergency coolant tank is filled up with water and the initial water level is below the inlet. Here the mixing of the injected water and the water in the tank is a point of interest if the temperatures or the boron concentrations are different. Another scenario for the occurrence of plunging jet phenomena can be found in the case of a break, when insulation material of components is released by the break. The fibrous material is transported into the reactor sump and might there perturb the core cooling system. During this situation the reactor sump is partially filled with water. The jet from the break impinges at the sump water surface and causes a fluid flow in the sump, which influences the transport of the fibrous insulation material towards the sump strainers. The gas entrainment and its influence on the fluid flow field and the transport of the fibrous insulation are of particular interest.

The focus of the present study is the carry-under of gas below the surface by the impinging jet. Several phenomena contribute to this effect. These phenomena are located inside the nozzle (generation of turbulence, development of the velocity profile), along the free falling jet (surface instabilities such surface waves, surface roughness) and at the point of impact, where bubbles are produced or not depending on the structure and the velocity of the jet.

The liquid flow inside the nozzle can be characterized by the liquid Reynolds number, based on the nozzle diameter. If the Reynolds number is low, the jet is laminar and a parabolic velocity profile develops inside cylindric nozzles. For high Reynolds numbers the jet is turbulent and the velocity profile is different. Only if the nozzle length l is large compared to the nozzle diameter d_0 the

velocity profile is fully developed at the nozzle exit. This is why the ratio l/d_0 affects the jet properties. After leaving the nozzle, the liquid does not experience the friction by the inner nozzle walls any more. Therefore a "relaxation" of the velocity profile starts. Below the nozzle the jet is surrounded by gas. So a free surface with a surface tension develops. The interaction of the jet with the gas can play an important role for the development of the jet.

Sleuyter (2004) identifies four different types of jet structures: If the jet is laminar, small disturbances can cause surface waves with a wavelength larger than the nozzle circumference. These waves propagate downwards. If their amplitude increases during this propagation, they lead to a breakup of the jet into drops with a diameter similar to the nozzle diameter. This phenomenon has been described by Rayleigh (1879) in a stability analysis. Therefore Sleuyter calls this jet behavior "Rayleigh flow regime". If the jet is faster, the aerodynamics of the gas around the jet becomes more important and causes the appearance of bulges (see figure 1c). This regime is called "first wind induced regime" by Sleuyter. In the "second wind induced regime" the surface of the jet is irregular, often described as "surface roughness". Droplets occur not far from the nozzle. For even higher velocities the jet breaks up into droplets (a spray) immediately below the nozzle. This is the "atomization regime".

The mechanism of gas entrainment at the jet impact point depends on the jet flow regime. If the jet is laminar and stable (no surface waves) the meniscus of the water is dented by the jet, but no bubbles appear below a certain critical impinging velocity. The lower rim of the dent has a radius r which depends on the jet velocity (figure 1a). This radius is proportional to exp(-Ca), with the capillary number $Ca = \eta v / \sigma$ (Lorenceau, 2007). Here η is the dynamic viscosity of the liquid, v the jet impact velocity and σ the surface tension. The capillary number indicates the ratio of the viscous force and the surface tension force. At high jet impact velocities (i.e. high capillary numbers), this proportionality is no longer valid and a thin gas film is transported below the water around the jet (figure 1b). At a certain depth the air film breaks up into bubbles. If the jet surface is unstable due to surface waves or surface roughness the gas film can also be fragmented by these instabilities (figure 1c by Ervine, 1987, see also Davoust, 2002).

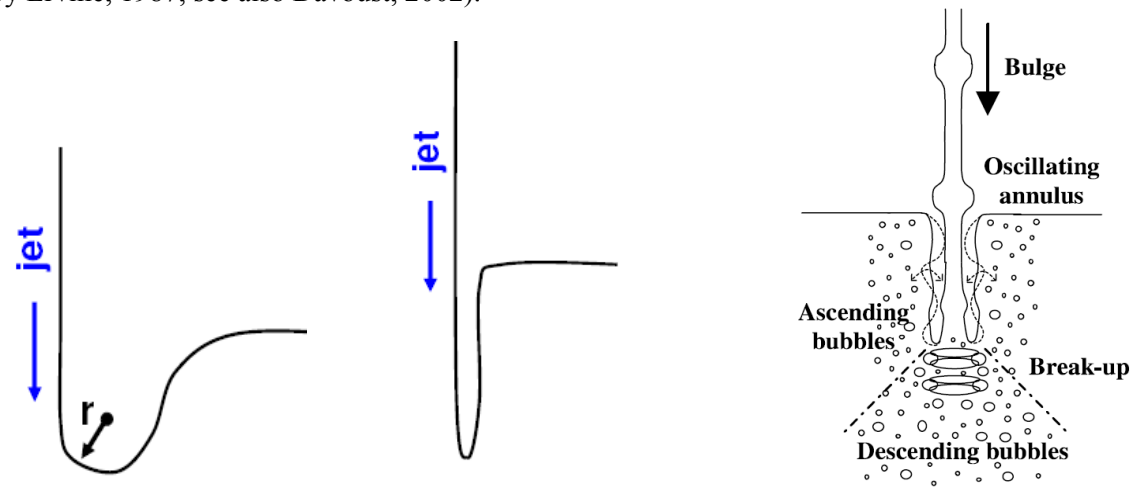

a) Low impact velocity: Jet dents the meniscus with radius r of lower rim

b) High impact velocity: Gas film transported below the water along the jet

c) First wind induced regime: Break-up of gas film triggered by surface instabilities (after Ervine, 1987)

Figure 1: Deformation of the water surface due to the jet impact.

As described above, many effects contribute to the gas entrainment by impinging jets. With the computational power available nowadays it is impossible to reproduce all these effects in one simulation: The interplay between turbulence inside the jet and surface instabilities at the jet surface can only be calculated, if the turbulence is resolved completely. For the reproduction of surface waves and gas film breakup the surface tension has to be calculated. This can only be done in a CFD simulation, if the interface is resolved in the whole domain. But this approach is not feasible if the surface structures are very small (due to surface roughness and gas film break up) and complex (e.g.due to a production and transport of many bubbles).

Generally for the CFD modeling of large hydrodynamic configurations with multiphase flow, the Euler-Euler approach is used. The physical process of bubble generation near a plunging jet occurs on a very small scale, which cannot be resolved in a meso-scale simulation. Therefore, the gas entrainment has to be physically modeled in simulations of plunging jets. The aim of this study is to find an approach for the simulation of plunging jet, where the gas entrainment can be deliberately tuned to some extent (e.g. in terms adjusting free parameters), in order for a physical model or correlation of the entrainment process to be implemented into future simulations.

In the plunging jet configuration, gas has two different morphologies The gas above the water level is a continuous phase, whereas the gas below the water level is bubbly, i.e. a dispersed phase. The water can be regarded as a continuous phase everywhere. For modelling this with the Euler-Euler method, two approaches are possible: One can use two different phases for the two morphologies of gas. Then water is treated as a third phase. Gas entrainment near the jet and degassing at the water surface has to be modelled with sources and sink terms that describes the conversion of gas from a continuous to a dispersed (bubbly) morphology and vice versa. This requires algorithms that identify the regions of entrainment and of degassing.

The other approach uses only two phases, one for water and one for gas. The different morphologies of the gas then have to be reflected by different coefficients in the closures for the momentum transfer between the gas and water phases. The first simulations presented here are performed with water as a continuous phase and gas as a dispersed phase. Thus, the gas is assumed to be bubbly everywhere in the domain, and a constant drag coefficient is applied. The influence of the magnitude of the drag coefficient is investigated. Then more complex drag model are tested, which take into account the different morphologies of the gas phase.

2. DEFINITION OF THE TEST CASE

2.1. Geometry and mesh

The geometry is a cylindrical tank with a diameter of 1 m. An inlet with a diameter of 19cm is located 2m above the tank bottom. The initial water level is 1.5m above the bottom. The jet diameter and height are similar to the configuration in which an emergency core coolant tank is filled (see introduction). A water outlet is at the side wall of the tank below the water surface. Presuming an axis-symmetric solution, only a sector of five degrees is modelled. The structured mesh has 125 uniform cells for the total height of the domain. For the radius of the water inlet seven uniform cells are used and 30 uniform cells for the opening (see figure 2). The tank is quite small compared to the jet diameter and the height of the water and the water in the tank is not very deep so that physicality of the result (particularly the development of the flow structures below the water level) is influenced significantly by the walls. This disadvantage is accepted, since we concentrate here on the gas entrainment, which takes place where the jet hits the water surface. It can be assumed that effects far away from this area do not influence the gas entrainment.
Of course it is possible use geometries and setups similar to experiments like Bonetto (1993). But this leads to more complex geometries and meshes. On the other hand, it is not clear, which approaches are feasible for modelling impinging jets at all. The simplicity of the geometry is accepted here since this investigation is meant to study concepts for modelling the gas entrainment. The limitations of the geometry and the low mesh resolution are meant to reduce the computational costs. This is important for parametric studies. For some of the cases the grid is refined by reducing the cell size by a factor two in each dimension to check the sensitivity of the results on the resolution.

2.2. Fluid properties, boundary conditions and turbulence modelling

During the calculations, the fluids are water for the continuous phase and gas for the dispersed bubbly phase. The main properties (at 25°C and atmospheric pressure) for water and gas (air) are summarized in table 1.

Property	Water	Gas (Air)
Viscosity ($kg \cdot m^{-1} \cdot s^{-1}$)	0.0008899	1.831e-05
Density ($kg \cdot m^{-3}$)	997	1.185

Table 1: Fluid properties

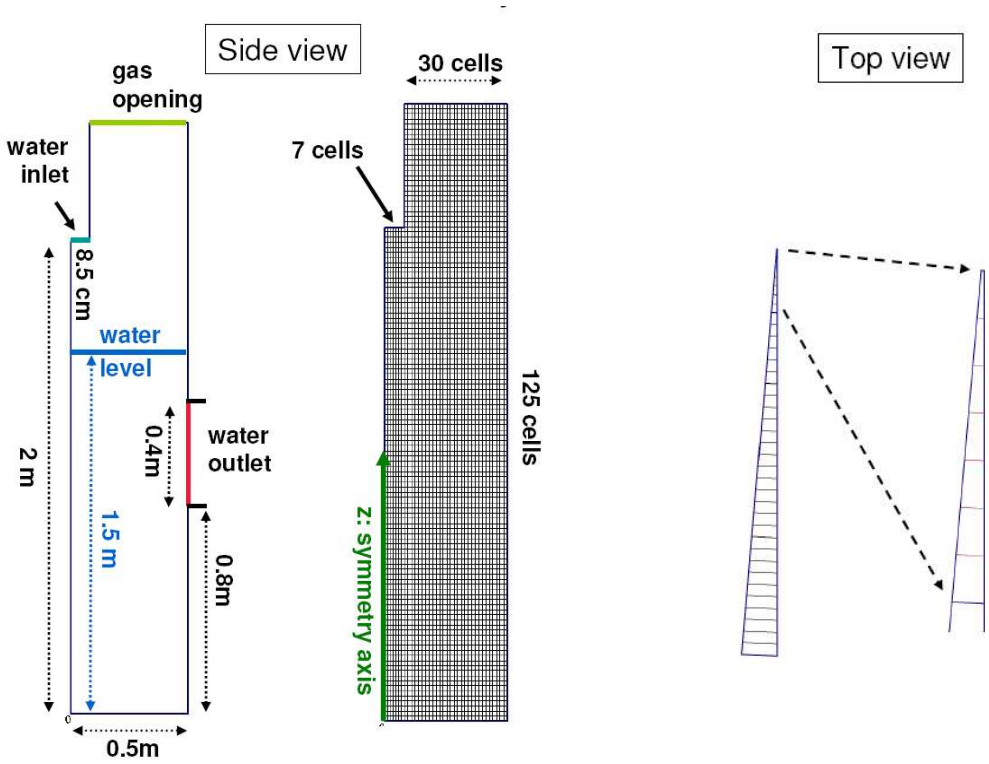

Figure 2: Section (five degrees) of the cylindrical tank; geometry and mesh.

The domain is partially filled with water up to a level of 150 cm above the bottom. The distance between the free surface and the water nozzle is then equal to 50 cm. The initial velocity for both water and gas in the computational domain are taken equal to 0 m/s in each direction. The hydrostatic pressure is initialized according to the water level in the domain.
The jet is injected through the nozzle with a velocity of 3 m/s. The volume fraction is 1 for water and 0 for gas. For the gas outlet, an opening condition is used. The volume fraction is 1 for gas and 0 for water. A constant relative pressure equal to 0 Pa is assumed. For the fluid, a velocity normal to the boundary condition is considered. For the liquid outlet, an outlet condition is used. The volume fraction is 1 for water and 0 for gas. Therefore, the gas mass flow rate is equal to 0 kg/s at this boundary condition. For the maintenance of a constant liquid level, the liquid mass flow rate leaving the domain is defined equal to the liquid mass flow rate introduced by the injector. Outer walls are defined using a no slip boundary condition. For the "inner walls" caused by limiting the domain to a section, a symmetry boundary condition is applied. In the case of stratified flows the buoyancy force causes a separation of gas and water.

2.3. Turbulence modelling

The homogeneous SST (shear stress turbulence) model is applied (i.e. no separate calculation of the turbulence for both phases). In the ANSYS CFX11-Solver modelling guide a homogeneous turbulence model is recommended for separate flow and stratified flow, whereas for dilute dispersed two-phase flow (e.g. bubbly flow) the manual recommends the use separate of turbulence models for each phase. In the plunging jet separate flow and bubbly flow coexist in one domain, so none of the turbulence

approaches is suitable everywhere in the domain. The calculations presented below are calculated with a homogeneous SST model by default. For comparison, some calculations were performed with an inhomogeneous turbulence model, which is the SST model for the liquid phase and a laminar assumption for the gaseous phase. The results were very similar to the calculations with the homogenous SST model. The applied numerical schemes are the "upwind" advection scheme and the "first order backward euler" transient scheme.

3. DISPERSED PHASE MODEL FOR GAS

The simplest approach for modelling the plunging jet, is if the water is treated as continuous phase and the gas is a dispersed phase with a constant particle diameter (d=2 mm) Bonetto observes bubbles with diameters between 1 and 3 mm. Due to equation (4.1) and (4.2) a variation of the particle diameter has the same effect as a variation of the drag coefficient of the dispersed phase (which is done below). Of course, the particle model is not appropriate for the gas above the water level. For the bubbles, a constant drag coefficient is used. The default value used here is C_D=0.44, which is the drag coefficient for solid spheres in the Newtonian range where C_D does not depend on the Reynolds number. To study the effect of the particle drag coefficient on the gas entrainment, the drag coefficient the simulations are performed with C_D=0.44 and with a reduced value C_D=0.05 for comparison.

Since the focus of this study is on the gas entrainment at the surface, non-drag forces (lift force and turbulent dispersion force) are neglected here. It is expected that the turbulent dispersion force causes an increase the horizontal extension of the bubble plume. Nevertheless, an application of non-drag forces above the water level is meaningless. Therefore, non-drag forces are not modelled here.
A few seconds after the jet release from the nozzle the interface becomes stable and the gas void fraction field also becomes steady (see figure 3). A reduction of the drag coefficient from C_D= 0.44 to C_D= 0.05 has no significant effect on the gas void fraction field. Thus, the drag coefficient cannot be used as a parameter influence the gas entrainment in the simulation. If the SST model is applied for the liquid phase and the turbulence of the gas is neglected (laminar assumption) the gas void fractions are similar to those in figure 3 which have been calculated with a homogenous SST model. Therefore, the coupling of both phases by sharing the same turbulence field does not contribute to gas entrainment. In the subsequent simulations, only the homogenous SST model is used.

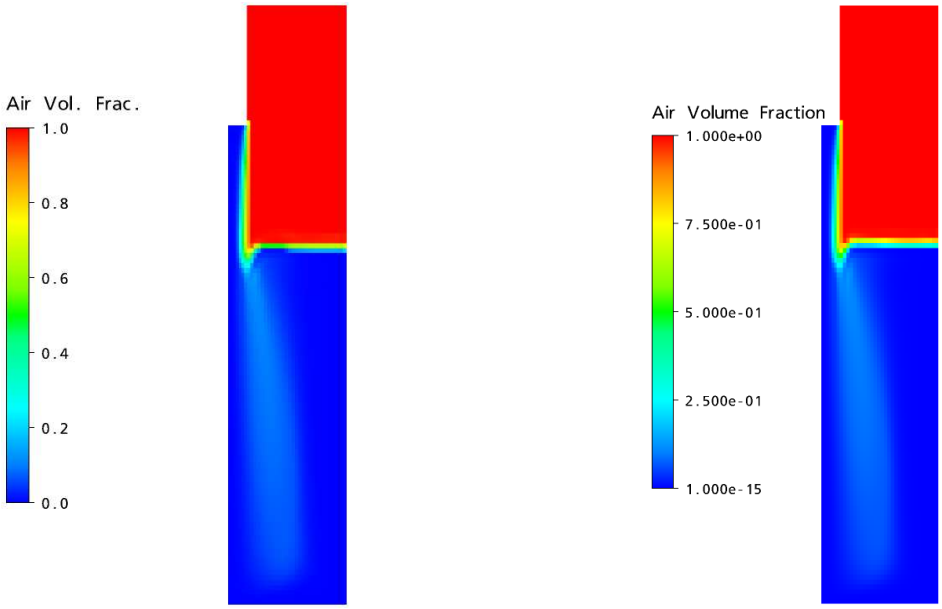

C_D= 0.44 C_D= 0.05

Figure 3: Gas void fraction fields for a simulation using a dispersed phase model for gas homogenous SST turbulence for both phases

For a characterization of the gas entrainment, it is advantageous to use integral quantities for the intensity and the geometry of the gas plume. By performing an extensive survey of experimental

studies Bin (1993) obtained correlations for the penetration depth and the entrainment rate. The penetration depth h_p is the vertical extension of the gas plume below the water level. Bin's correlation for the penetration depth in meter is

$$h_p = 2.1\, w_j^{\,0.775}\, d_0^{\,0.67}, \tag{3.1}$$

where d_0 is the nozzle diameter in meter and w_j is the vertical jet velocity at the water level (in m/s). Due to gravitational acceleration, the velocity of a free falling jet increasing until it hits the surface. If h_j is the height of the nozzle above the surface and w_0 is the liquid velocity at the nozzle w_j can be calculated as

$$w_j = \sqrt{w_0^2 + 2g\, h_j} \tag{3.2}$$

For the height of h_j = 0.5 and w_0 =3.0 m/s, one obtains w_j = 4.3 m/s for the jet velocity at the water level and a penetration depth of 2.15 m according equation (3.1). The predicted value for the penetration depth is larger then the depth of the water in the tank. Therefore, the length of the gas plume might be restricted artificially by the geometry. In fact, according to figure 4 the gas plumes almost reach the bottom of the tank. For a better quantification of the vertical distribution of the gas, the gas void fraction α_G is integrated on horizontal planes.

$$A_G = \int_A \alpha_G \, dA \tag{3.3}$$

Since the gas void fraction is dimensionless, the integral (3.3) yields the dimension of an area for A_G. This can be interpreted as the area occupied by gas on the horizontal plane A. In figure 4 A_G is plotted versus the depth below the water level. Here A_G is normalized by the area of the jet cross section at the inlet. There is only a little difference between the values for C_D=0.44 and C_D=0.05 (see also Figure 3). The axial water velocities are identical for both drag coefficients.

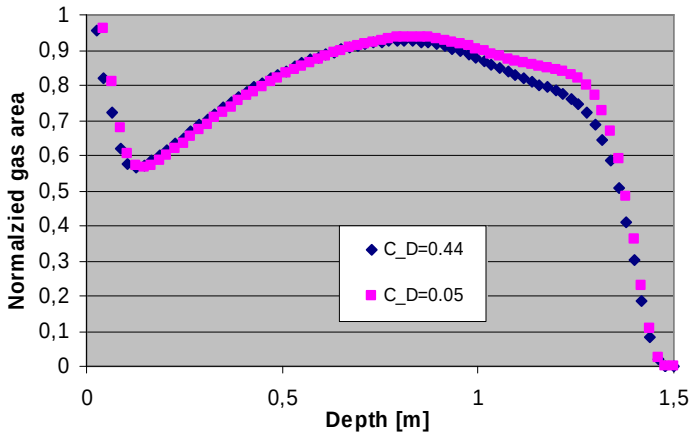

Figure 4: Normalized gas area as a function of the depth below the water surface

The depth at which the normalized gas area is zero can be used to define a penetration depth for jets. According to figure 4 the penetration depth almost 1.5 m which means that the plumes reach the tank bottom. This is in accordance with the prediction of equation (3.1).
The entrainment rate is the ratio of the gas flux Q_G entrained below the water by the impinging jet and the water flux Q_L of the jet. The correlation for the entrainment rate suggested by Bin (1993) is

$$\frac{Q_G}{Q_L} = 0.04\, Fr^{0.28} \left(\frac{h_j}{d_0} \right)^{0.4}, \qquad \text{with} \qquad Fr = \frac{w_j^2}{g\, d_0}. \tag{3.4}$$

where h_j is the jet height above the water level and g is the gravity. For the boundary conditions used in the simulations, this correlation yields an entrainment rate of 0.08. Another correlation was obtained by Ohkawa et al (1986) :

$$\frac{Q_G}{Q_L} = 0.016\left[Fr^{0.28}\left(\frac{h_j}{d_0}\right)^{0.4}\right]^{1.17} \tag{3.5}$$

This correlation yields an entrainment rate of 0.036 in for the boundary conditions used here. To compare the simulation results in terms of entrainment rate with the predictions given by correlations (3.4) and (3.5), the gas fluxes below the water have to be investigated more closely. The product of the gas void fraction α_G and the vertical velocity of the gas w_G defines a vertical gas flux density q_G :

$$q_G = \alpha_G w_G \tag{3.6}$$

The upward and the downward fluxes can be distinguished by the definition of

$$q_G^+ = \begin{cases} q_G & \text{if } q_G > 0 \\ 0 & \text{else.} \end{cases} \quad \text{and} \quad q_G^- = \begin{cases} q_G & \text{if } q_G < 0 \\ 0 & \text{else.} \end{cases} \tag{3.7}$$

So the total downward flux at a certain level below the surface is

$$Q_G^- = \int_A q_G^- \, dA, \tag{3.8}$$

where A is the horizontal cross section of the domain at a certain level below the surface. The total upward flux Q_G^+ is calculated in the same way.

In figure 5 the total upward and downward gas fluxes are shown for the two jets modelled with the drag coefficients C_D=0.44 and C_D=0.05. The gas fluxes below the water level are normalized by the water flux of the jet $Q_{L,0}$ at the nozzle and plotted as function of the depth below the water level. For C_D=0.44 the upward and downward gas fluxes are similar which means that the solution is steady: At each level the same amount is transported upwards and downwards. For the different drag coefficients the gas downward fluxes are also similar. Thus, the drag hardly contributes to gas entrainment. The carry under of gas therefore seems to be mainly caused by numerical effects within the solver. The curves for the normalized gas fluxes show a local minimum ca. 10 cm below the water level. This is the depth of the deformed water surface ("trumpet") near the jet. At a depth of 60 cm all the curves have a local maximum. This can be explained by the re-entrainment of bubbles, which are trapped in the vortex caused by the jet. At the depth of 20cm the normalized gas fluxes are about 0.06 which is just between the predictions for the entrainment rate by Bin (eqn. 3.4) and by Ohkawa (eqn 3.5). Since the entrainment is mainly caused by numerical effects in this setup, we can expect the value to be sensitive to the geometry and resolution of the grid. This must be studied in future. However, it seems to be a coincidence that the simulated entrainment rate in this simulation is in the range predicted by empirical correlations.

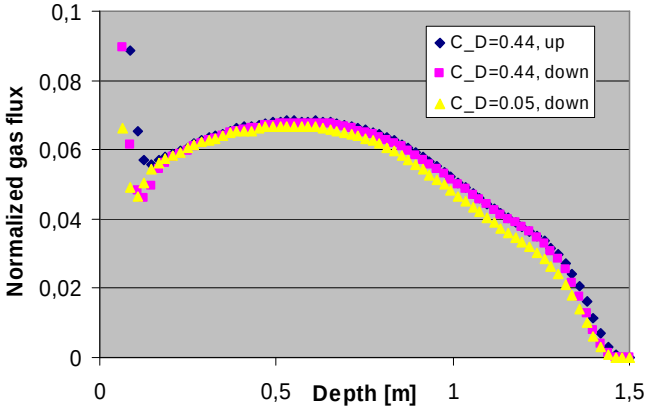

Figure 5: Normalized gas fluxes as function of the depth below the water level. Blue symbols: Upward gas flux (C_D=0.44). Red symbols: Downward gas flux (C_D=0.44). Yellow: Downward gas flux (C_D=0.05)

4. The algebraic interfacial area density drag model

In the previous simulations the gas was treated as a dispersed phase everywhere in the domain. However, the algebraic interfacial area density model (AIAD) model takes into account the distinction in morphology that phases can have in the domain. The morphology of the phases has to be reflected by appropriate parameters in the drag force. The magnitude of the force density for the drag is

$$| D | = C_D \, a \frac{1}{2} \rho \left| \mathbf{V_R} \right|^2 \tag{4.1}$$

where C_D is the drag coefficient, a the interfacial area density and ρ the density of the continuous phase (if the other phase is a dispersed phase). $\mathbf{V}_R$ is the relative velocity between the two phases.
The algebraic interfacial area density model applies two different drag coefficients, $C_{D,B}$ for bubbles and $C_{D,S}$ for free surface. The interfacial area density a also depends on the morphology of the phases. For bubbles it is

$$a_B = \frac{1}{4} \frac{6}{d_B} \alpha_G \tag{4.2}$$

where d_B is the bubble diameter and α_G is the gas void fraction. If a free surface is fully resolved, its interfacial area density is

$$a_S = | \nabla \alpha_G | \tag{4.3}$$

Since the concept of a continuous phase is not meaningful in the range of medium gas void fractions, instead of a continuous phase density an average density is applied in equation (3.1). The average density is defined as

$$\rho = \rho_G \, \alpha_G + \rho_L \, (1 - \alpha_G) \tag{4.4}$$

where ρ_L and ρ_G are the liquid and the gas phase density respectively. In the bubbly regime, where α_G is low, the average density according to equation (4.4) is close to the liquid phase density ρ_L, which is the continuous phase density in this case. According to the flow regime (bubbly flow or stratified flow with a free surface) the corresponding drag coefficients and interfacial area densities have to be applied. This can be done by introducing a blending function f which is 1 for bubbly flow and 0 for stratified flow. Then the area density and the drag coefficient are well defined everywhere in the domain by

$$a = f \, a_B + (1 - f) \, a_S \tag{4.5}$$

$$C_D = f \, C_{D,B} + (1 - f) \, C_{D,S} \tag{4.6}$$

It is not easy to find an algorithm that recognizes the flow regime of course. A very simple approach identifies the flow regime by using a gas void fraction limit α_0. Bubbly flow is assumed, where $\alpha_G < \alpha_0$ and stratified flow everywhere else. This would mean that blending function f is a step function. To avoid numerical problems a continuous blending function is preferred (figure 6):

$$f = \frac{1}{1 + \exp(-100 \, (\alpha_G - \alpha_0))} \tag{4.7}$$

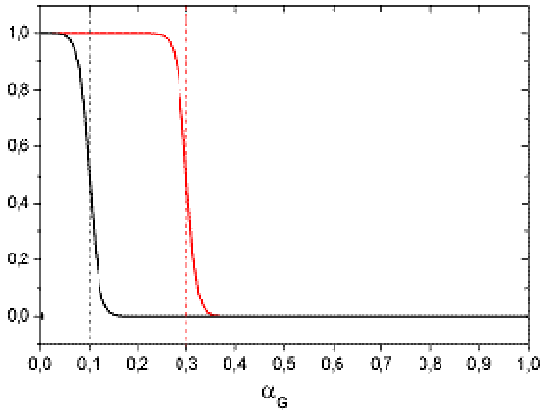

Figure 6: Blending function f according to equation (3.7) for α_0= 0.1 (black curve) and α_0 = 0.3 (red).

For a first judgement, the gas entrainment is quantified by the gas void fractions just below the liquid interface. These are investigated for various values of the free surface drag coefficient $C_{D,S}$ and gas void fraction limits α_0. For the bubble drag coefficient, a constant value of $C_{D,B}$ = 0.44 is taken, based on the drag of rigid spheres at the medium to high Reynolds number regime. As bubble diameter d_B=2mm is chosen.

4.1. Variation of the surface drag coefficient

Figure 7a shows the gas void fraction for $C_{D,S}$ = 10. The gas entrainment seems to be overestimated here, since even at a depth of 50cm below the water surface gas void fractions of 0.5 appear. In figure 7b the corresponding bubble area density a_B is displayed. Note that a_B is proportional to the gas void fraction (eqn. 3.2) and maximal at α_G = 1 (figure 7b). Of course bubbles are not assumed to be present where α_G = 1. According to equation (4.5) and (4.7) the blending function switches to free surface area density a_S at high gas void fractions. The free surface area density a_S for this case is shown in figure 7c. In figure 8 the total area density a according to equation (4.5), the total drag coefficient C_D according to equation (4.6) and the product of a and C_D are shown.

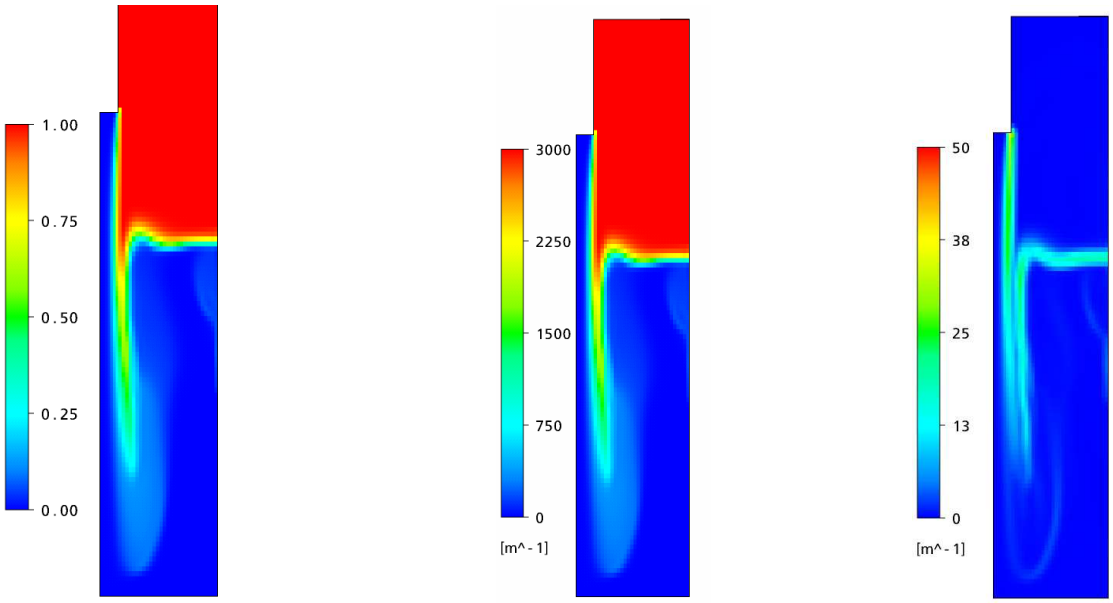

a: Gas void fraction α_G b : Bubble area density a_B c: Free surface area density a_S

Figure 7: Various scalar fields for a simulation with $C_{D,S}$ = 10.

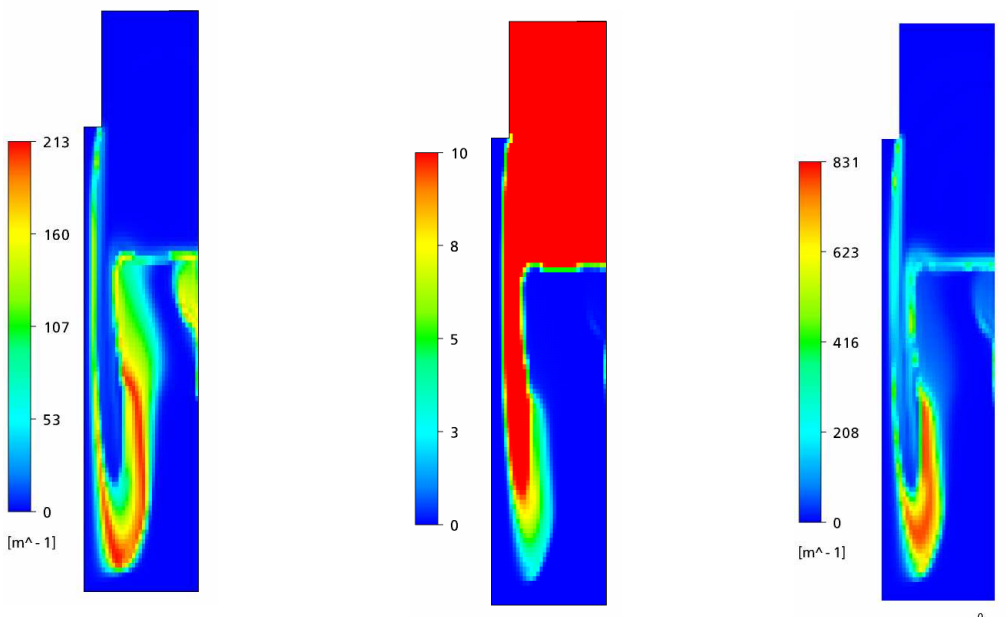

a: Total area density a b: Total drag coeff. C_D c: Product $a\ C_D$

Figure 8: Various scalar fields for a simulation with $C_{D,S} = 10$.

It is not clear which surface drag coefficient is appropriate for the situation of the impinging jet. The value of $C_{D,S}$ has to include subgrid information of the free surface structure ("rough" or "smooth") and this certainly depends on the grid resolution, since with a finer mesh more details of the surface structure are resolved. Therefore, the free surface drag coefficient $C_{D,S}$ is varied over several orders of magnitude. Its influence on the gas void fraction below the water surface is studied while keeping the gas void fraction limit in equation (4.7) constant at $\alpha_0 = 0.1$. Note that the vertical water velocity at the nozzle is kept constant at $w_0 = 3$ m/s. The simulation is performed in the transient mode, but the result is almost in a steady state 10 seconds after the start when the jet is released from the nozzle.

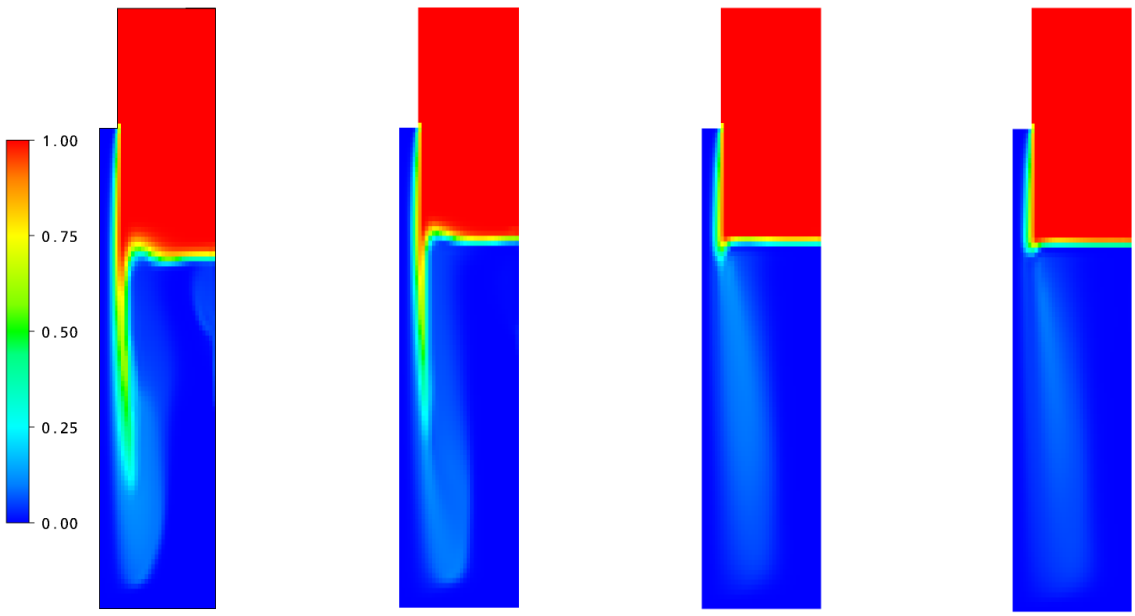

$C_{D,S} = 10$ $C_{D,S} = 1$ $C_{D,S} = 0.1$ $C_{D,S} = 0.01$

Figure 9: Gas void fraction for various surface drag coefficients. Representative plots at time t >10s.

As one can see from figure 9 the gas entrainment below the surface decreases if the surface drag coefficient is reduced. Note that the solver does not converge when $C_{D,S} = 0$. Since the maximal gas void fraction below the water surface is similar for $C_{D,S} = 0.1$ and $C_{D,S} = 0.01$ it is obvious that entrainment cannot be suppressed by further reducing $C_{D,S}$.

4.2. Variation of the blending function

By changing the gas void fraction limit α_0 the blending function can be modified. The value of α_0 has a significant influence on the gas entrainment (figure 10). It is not clear which value is appropriate since α_0 has no physical meaning. The definition of the blending function in general and of α_0 in particular is arbitrary to some extent. Note that in this case the gas void fraction α_G is used as criterion to identify the location of the surface. This is a quite simple approach of course and a more sophisticated blending function could use the gradient of α_G to identify the surface since this gradient is high near the surface.

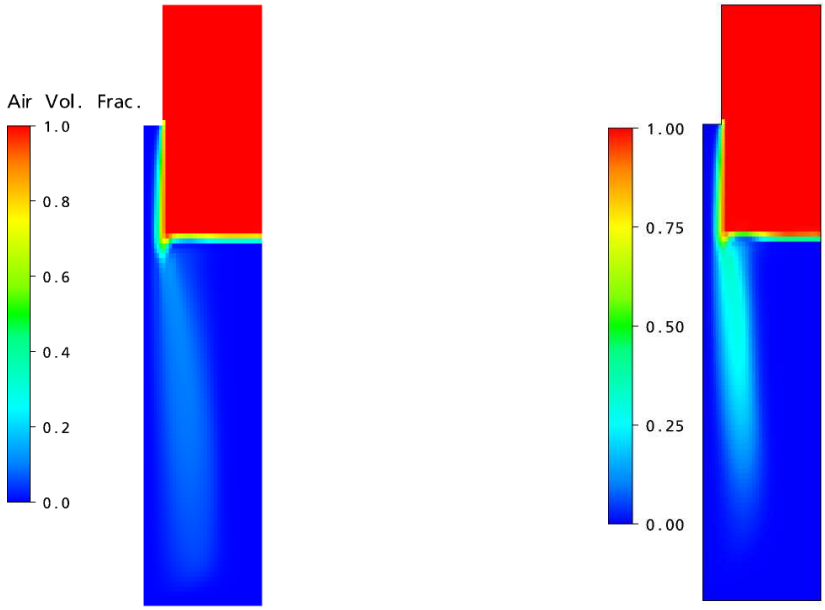

Figure 10: Gas void fraction for $C_{D,S} = 0.1$ and various α_0 .

To check the influence of the grid resolution on the numerical solution one calculation (C_D=0.1) is repeated with a doubled spatial resolution. The gas void fraction fields are similar. By an integration of the vertical flux density at this level according to equation (3.8) and by normalizing the result with the water flux at the nozzle $Q_{L,0}$ the dimensionless entrainment rate is obtained. For the coarse mesh the entrainment rate is 3.5% and for the fine mesh it is about 6.4%. Of course the results of a CFD model should not depend on the resolution of a grid (Menter, 2002). However, in a simulation of an impinging jet with increasing resolution increasingly of the complex geometry of the impinging zone is resolved. In the borderline case of an infinite resolution the real bubble generation process could be captured. With a decreasing resolution, the geometry of the impinging zone is further simplified. This is the reason why the resolution has an effect on the simulated entrainment.

5. Conclusion

For the implementation of a physical model for the gas entrainment by impinging jets in the frame of a CFD code, a mechanism is required that allows the adjustment of the entrainment in the simulation according to the correlation. Since the gas and liquid phase tend to separate due to the buoyancy force, it is obvious to use its counterpart – the drag force – to obtain gas entrainment below the surface. However, if the gas is modeled as dispersed phase in an Euler-Euler simulation, the entrainment barely

depends on the magnitude of drag coefficient, and it is obviously caused by numerical effects. Thus, this approach is not suitable for the implementation of a physical model for gas entrainment.

The algebraic interfacial area density (AIAD) model was found to be a suitable approach to adjust the entrainment. There are two free parameters inside the AIAD model have a strong influence on the suction of gas across the liquid interface. These parameters are a drag coefficient for the free surface and the shape of the blending function. The blending function is used to identify regions of stratified flow (free surface flow) and regions of dispersed phase flow (bubbly flow) in order to apply the appropriate drag model. Nevertheless, the gas entrainment calculated with the AIAD model is arbitrary, as the model does not realistically reflect physics of the bubble entrainment. Further investigations will be performed to improve the parameterization in terms of the AIAD model:

- In the AIAD model, only the magnitude of the gas void fraction is evaluated by the blending function to identify the location of the free surface. In a more sophisticated approach more criteria could be evaluated such as the gradient of the gas void fraction.
- It is not clear which drag coefficients for the free surface are appropriate. The drag coefficient should also reflect the roughness of the jet surface for example.
- In the present simulations the blending function is meant to identify the location of the free surface. With a more complex algorithm it might be possible to identify the region where the jet entrains gas. This would allow applying special closure models (e.g. drag forces) to obtain a more controlled gas entrainment there.
- The parameters for a realistic entrainment probably depend on the grid resolution.
- Up to now the literature about gas entrainment near impinging jets is rather fragmentary. More experimental data are necessary to adjust the CFD models and obtain realistic entrainment in simulations. The Forschungszentrum Dresden-Rossendorf (FZD) is planning to perform new experiments with impinging jets. New sensors for multiphase flow measurements, which have been developed at the FZD, will also be used.

ACKNOWLEDGEMENTS

The present work has been done in the frame of the NURESIM project, is partly funded by the European Commission in the framework of the Sixth Framework Program (2004-2006), Contract Nr. 516560 (FI6O).

REFERENCES

ANSYS CFX-Solver Modeling Guide, ANSYS CFX Release 11.0

Bin, A.K.: “Gas Entrainment by plunging liquid jets”, *Chem. Eng. Sci*, Vol. 48, No. 21, pp. 3585-3630, (1993)

Bonetto, F.; Lahey, R.T. Jr.: “An experimental study on air carryunder due to a plunging liquid jet”, *Int. J. of Multiphase Flows*, 19, pp. 281-294 (1993).

Davoust, L; Achard, J.L. El Hammoumi, M: “Air entrainment by a plunging jet: the dynamical roughness concept ant its estimation by a light absorption technique” *Int. J. Multiphase Flow* 28, pp.1541-1564 (2002).

Lorenceau, É.; Reyssat, É. Restagno, F; Eggers, J. Quéré, D: “On liquid/liquid impact”, *6th Int. Conference on Multiphase Flow, ICMF 2007*, Leipzig, Germany (2007)

Menter,F.R.: “CFD Best Practice Guidelines for CFD Code Validation for Reactor-Safety Applications”, *ECORA, Deliverable Report EVOL-ECORA-D01* (2002).

Rayleigh, J.W.S: “On the Instability of Jets” *Proc. London Math. Soc*. 10, pp.4-13, (1879).

Ohkawa, A; Kusabiraki, D.; Kawai, Y.; Sakai, N: „Some flow characterisitics of a vertical liquid jet system having downcomers“, *Chem. Eng. Sci*, No 41, pp. 2347-2361 (1986).

Sleuter, F.C.B.: “Stability of flashing and non-flashing liquid jets” *Master thesis*, Technische Universiteit Eindhoven (2004).